

RESEARCH

Open Access



# Experimental and Theoretical Study of Concrete-Filled Steel Tube Columns Strengthened by FRP/Steel Strips Under Axial Compression

Shichang Zhang<sup>1,3\*</sup>, Kunting Miao<sup>2\*</sup>, Yang Wei<sup>2\*</sup> , Xiaoming Xu<sup>3</sup>, Bin Luo<sup>1</sup> and Weizhou Shi<sup>3</sup>

## Abstract

Concrete-filled steel tube (CFST) columns are widely used in civil engineering because of their excellent bearing capacity; however, the reinforcement of CFST columns lacks effective measures. To strengthen CFST columns quickly and effectively, two methods, namely, winding FRP (fiber reinforced polymer) or steel strips, were explored in this work. Two unconfined CFST columns, eight FRP-strengthened CFST columns and four welded steel strip-strengthened CFST columns were manufactured and tested. The failure modes and axial load–strain curves of all specimens under compression load were concluded and compared. The effects of the primary parameters, such as FRP layers (1, 2, 3 and 4 layers) and steel strip thickness (3.0 and 6.0 mm), on the bearing capacity and deformation capacity were also investigated. The ultimate load of CFST columns increased from 28.72 to 64.16% after being confined by FRP with one to four layers. The ultimate load of the welded steel strip-strengthened CFST column with 3.0 mm steel strips and 6.0 mm steel strips increased by 28.46% and 49.82%, respectively, compared with the unconfined CFST column. Thus, the increase in FRP layers and steel strip thickness can markedly improve the compressive behavior of the FRP/welded steel strip-strengthened CFST columns. The cost performance of the two different reinforcement methods also showed that the cost of the welded steel strip-strengthened CFST column is nearly 40% of that of the FRP-strengthened CFST column when the same strengthening effect was obtained, which indicated that the welded steel strip-strengthened CFST column is more cost-efficient than CFST columns confined by FRP. Finally, six existing models for the ultimate load of FRP-strengthened CFST columns were presented and evaluated. From the evaluation results, the Zhang et al.'s model, Lu et al.'s model and Hu et al.'s model for FRP-strengthened CFST columns were shown to provide the best applicability and accuracy. Based on the Mander et al.'s model, a model for the ultimate load of welded steel strip-strengthened CFST columns was proposed and evaluated. The proposed model can accurately predict the ultimate load of welded steel strip-strengthened CFST columns.

**Keywords:** Concrete-filled steel tube, Fiber reinforced polymer, Steel strip, Compression behavior, Ultimate load model

Journal information: ISSN 1976-0485 / eISSN 2234-1315.

\*Correspondence: zhangsc@isaarchitecture.com; mkt97@njfu.edu.cn; wy78@njfu.edu.cn

<sup>1</sup> Southeast University, Nanjing 210096, China

<sup>2</sup> College of Civil Engineering, Nanjing Forestry University, Nanjing 210037, China

Full list of author information is available at the end of the article

## 1 Introduction

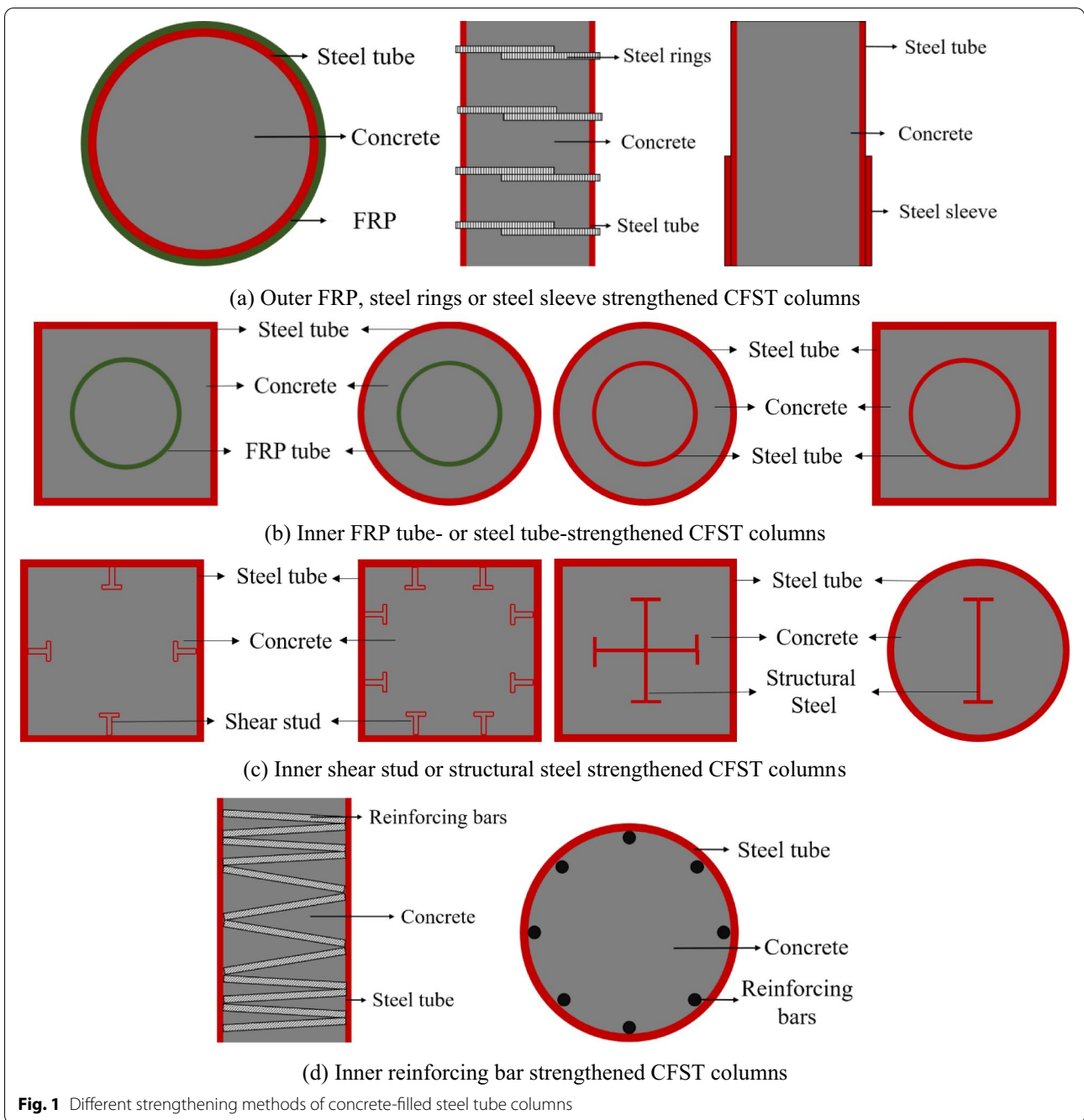
In the field of civil engineering, concrete and steel are the most widely used and most demanding foundation engineering materials. Since the invention of Portland cement in 1824, concrete has begun to become the most common material in civil engineering. The mechanical performance of concrete has also been studied by many

scholars, which shows that the bearing capacity and deformation of the structure are improved effectively when the concrete is in the state of triaxial compression (Ahmed et al., 2020; Wang et al., 2020; Wei et al., 2019a; Zheng & Wang, 2017). Concurrently, due to the superior tensile performance and energy dissipation of steel, the concrete-filled steel tube (CFST) column structure began to be investigated and applied in the middle of the nineteenth century (Stephens et al., 2018; Wang et al., 2022; Wei et al., 2022a; Zeng et al., 2017; Zong et al., 2005). The earliest engineering application of this structure was the pier of Severn Railway Bridge built in 1879 in the UK (Bradley & Roberts, 2010). Numerous engineering practices have shown that pouring concrete in steel tubes can improve the bearing capacity of the structure and effectively prevent the buckling and corrosion of the inner face of steel tubes (Chin et al., 2019; Wei et al., 2019b; Zhang et al., 2020b). However, the CFST column structure also has disadvantages, such as poor durability and local buckling.

In the service process of CFST column structures, local corrosion and concrete cavitation often occur due to external actions, such as long-term loading and environmental corrosion, or internal action, such as concrete shrinkage and creep. Many scholars have investigated the influence of various defects on CFST structures (Han et al., 2012; Hou et al., 2016; Liao et al., 2011, 2013; Xu et al., 2017; Zhang et al., 2020a, 2021). Han et al. (2012) conducted an experimental study on square CFST columns under the conditions of long-term loading or chloride ion corrosion and concluded that the influence of long-term loading and chloride ion corrosion on CFST columns is high: the ductility and bearing capacity of CFST columns decreased by 29.8% and 31.7%, respectively. Liao et al. (2011) performed an experimental study on CFST columns and CFST beams with initial concrete imperfections, and their test results showed that the bearing capacity of CFST columns decreased by 23% and 29% when the gap ratio reached 1.1% and 2.2%, respectively. The deformation capacity of CFST beams decreased by 13% and 34% when the gap ratio reached 1.1% and 2.2%, respectively. Defects such as concrete cavitation and local corrosion can thus markedly weaken the performance and durability of CFST structures, which could lead to serious security incidents. In addition, in reconstruction and expansion projects, the bearing capacity of the original CFST column structure is typically insufficient to support the new structure. In new construction, defects in CFST structures are often found during completion acceptance, because the construction technology level and the project management are not standard. Thus, it is critical to investigate the reinforcement measures of CFST structures.

Currently, the strengthening structural measures of CFST columns can be divided into two categories (Zhang & Zhang, 2015): strengthening structural measures outside the CFST columns (Fig. 1a) and strengthening structural measures inside the CFST columns (Fig. 1b–d). The most common strengthening structural measures outside CFST columns are welding steel members, pasting FRP and so on (Choi & Yan, 2010; Alrebeh & Ekmekyapar, 2019; Lai & Ho, 2014a; Lai & Ho, 2015; Lai & Ho, 2014b; Na et al., 2018; Tang et al., 2020; Wang et al., 2021; Wei et al.; Zhang et al., 2020b). To improve the interface bonding between the steel tube and concrete, reinforcing rings and internal stiffening using reinforcing bars strengthening CFST columns were proposed by Alrebeh et al. (2019). The test results showed that compared with CFST columns confined singly by external reinforcing rings and internal reinforcing bars, this new structure can provide better reinforcement. Wang et al. (2021) performed a theoretical study of the performance of CFRP-strengthened CFST columns under compression bending–torsion loading. The test results showed that the bearing capacity, deformation ability and ductility improved due to the confinement provided by FRP. Lai et al. (2014a) proposed a structure called ring-confined CFST columns. The mechanical properties of this structure under uniaxial loading were also investigated. The test results showed that the bearing capacity and stiffness of CFST columns improved, and the strength degradation rate decreased due to the existence of a ring. The failure mode also changed from end failure to buckling between the steel rings.

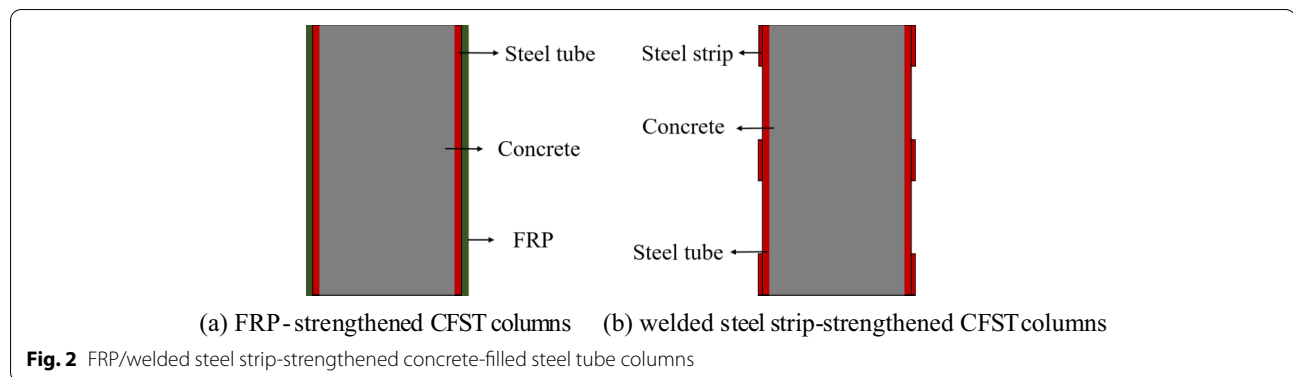
The most common strengthening structural measures inside CFST columns are setting up stirrups, inner FRP tubes, and inner steel members (Ding et al., 2020; Ekmekyapar & Alhatmey, 2019; Feng et al., 2015; Hu et al., 2020; Wang et al., 2019; Wei et al.). Ding et al. (2020) proposed strengthening CFST columns by installing stirrup cages inside the CFST columns. The effect of the contact mode between the stirrup cage and steel tube on the structural performance was investigated with cyclic loading tests on this new structure. The test results showed that the stirrup cage markedly improves the seismic performance of CFST columns. In addition, the square CFST column achieves better performance than the circular CFST column. Ekmekyapar et al. (2019) investigated the post fire resistance of internally ring-stiffened high-performance concrete-filled steel tube columns. The test results showed that the internal ring effectively improved the carrying capacity and fire resistance of the structure but had little impact on the failure mode. Feng et al. (2015) conducted an axial compression test on 18 square double-skin tubular columns with concrete-filled inner tubes. The effects of the concrete strength, number



of layers of FRP tubes and thickness of steel tubes on the mechanical behavior of this structure were investigated. The test results showed that the square double-skin tubular columns with concrete-filled inner tubes exhibited better residual load-bearing capacity and ductility.

In the above studies, most of the reinforcement methods are used to strengthen new CFT columns, and the reinforcing parts are located inside the steel tube, so these methods cannot be used to reinforce existing CFST

columns. Research on FRP, steel rings or steel sleeve strengthened CFST columns was only carried out on small members, and the implementation effectiveness of the construction technology needs further demonstration. In view of practical CFT columns, large-scale model tests for the two reinforcement methods were conducted, and different methods were compared in terms of cost performance and construction technology in this study. Fourteen CFST column specimens were made and tested,

**Table 1** FRP-strengthened CFST columns

Specimens	Diameter/mm	Height/mm	Steel tube thickness/ mm	FRP layers	FRP type	Number of specimen
C0CFST	159	636	4.0	0	/	2
C1CFST	159	636	4.0	1	CFRP	2
C2CFST	159	636	4.0	2	CFRP	2
C3CFST	159	636	4.0	3	CFRP	2
C4CFST	159	636	4.0	4	CFRP	2

including two ordinary CFST column specimens, eight FRP-strengthened CFST column specimens (Fig. 2a) and four welded steel strip-strengthened CFST column specimens (Fig. 2b). Based on the test results, the failure modes and axial load–strain curves of FRP-strengthened CFST columns and welded steel strip-strengthened CFST columns were summarized and compared. The cost/increase of the ultimate load of the two reinforcement methods was also investigated to provide a reference for the comparison and selection of reinforcement methods in engineering practice. Finally, the existing calculation model for the bearing capacity of FRP-strengthened CFST columns was summarized and evaluated. A model for the ultimate load of welded steel strip-strengthened CFST columns was also proposed.

## 2 Experimental Program

### 2.1 Specimen Design

In this study, 14 concrete-filled steel tube (CFST) columns were designed and manufactured in 7 groups with different parameters (two specimens were designed for each same parameter), two of which were unconfined CFST columns, eight of which were FRP-strengthened CFST columns and four of which were welded steel strip-strengthened CFST columns. Due to the superior ductility and bearing capacity of steel tubes, the brittleness of concrete has been greatly improved, and the difference in the mechanical properties of CFST structures

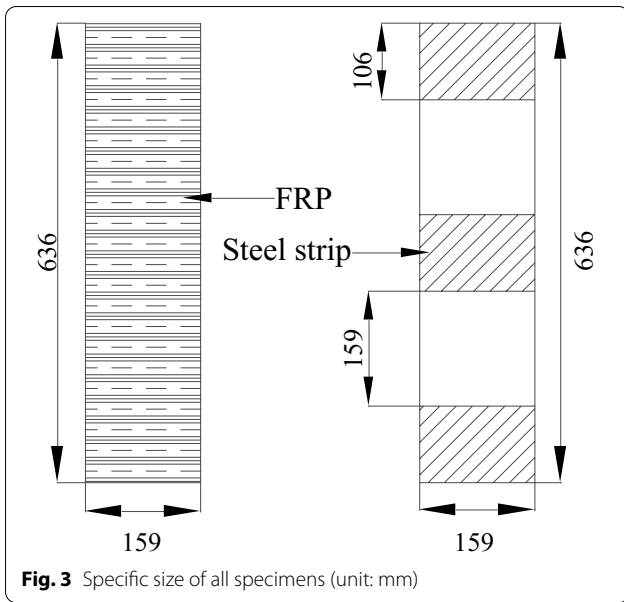
**Table 2** Welded steel strip-strengthened CFST columns

Specimens	Diameter/ mm	Height/ mm	Steel tube thickness/ mm	Steel strip thickness/ mm	Number of specimen
S3CFST	159	636	4.0	3.0	2
S6CFST	159	636	4.0	6.0	2

is rather small. Hence, two specimens were designed for each parameter (Yu et al., 2017; Zeng et al., 2018). The outer diameter of all specimens was 159 mm, the height was 636 mm, and the thickness of the steel tubes was 4.0 mm. The primary parameters were the number of FRP layers (1, 2, 3 and 4 layers) and the thickness of the steel strip (3.0 mm and 6.0 mm). The specific sizes of all specimens are shown in Tables 1 and 2 and Fig. 3. The naming rule of the specimens is as follows: “C0” denotes the layers of FRP, “CFST” denotes the concrete-filled steel tube columns, and “S3” denotes the thickness of the steel strip. For example, “C3CFST” represents a concrete-filled steel tube column confined by three layers of FRP, and “S3CFST” represents a concrete-filled steel tube column confined by a steel strip with a thickness of 3.0 mm.

### 2.2 Specimen Manufacture

As shown in Figs. 4, 5 and 6, the production process of FRP-strengthened CFST columns primarily includes the following three steps: treatment of the steel tube, pasting



FRP, and pouring concrete. The production process of welded steel strip-strengthened CFST columns primarily includes the following two steps: welding the steel strip and pouring the concrete. The specific steps are as follows:

(1) Treating the steel tube

All steel tubes used in this study are circular seamless steel tubes that were cut from the same batch by the manufacturer. Before pasting FRP and welding the steel strip, the steel tube should be polished by a grinder to clean the rust to ensure that the FRP

or steel strip is pasted tightly to the steel tube, as shown in Fig. 4a.

(2) Pasting the FRP/welding steel strip

FRP was pasted by the following steps: (a) FRP was cut to the corresponding length and width according to the layers of FRP; and (b) alcohol solution was used to wipe the steel tube to remove impurities on the surface of the steel tube. Then, epoxy resin adhesive was evenly applied on the outer wall of the steel tube (Fig. 4b). (c) Epoxy resin adhesive was applied evenly on both sides of the FRP and pressed repeatedly with a roller brush to fully impregnate it. Then, FRP was pasted onto the steel tube. First, one end of FRP was fixed on the steel tube. Then, the roller brush was used to repeatedly apply pressure to make the FRP fit. Concurrently, air bubbles were squeezed out along the winding direction (Fig. 4c). (d) After the epoxy resin adhesive cured, FRP pasting was completed (Fig. 4d). Because the width of the FRP is smaller than the height of the specimen, the FRP sheet was lap-wrapped.

The steel strip was welded by the following steps: (a) one end of the prepared steel strip was welded to the steel tube by the spot welding method (Fig. 5a); (b) a steel bar was welded to the other end of the steel strip to make it easier to bend (Fig. 5b); (c) the steel strip was bent with a steel bar and struck with a hammer to ensure that it was attached to the steel tube closely, and the welding gun was used for spot welding (Fig. 5c, d); and (d) when the steel strip was completely attached to the steel tube, the





(a) Weld one end of the steel strip



(b) Weld steel bar to the other end of the steel strip



(c) Bend steel strip



(d) Spot weld steel strip



(e) Overall welding of steel strip



(f) CFST columns confined by steel strip

**Fig. 5** Production process of welded steel strip-strengthened CFST columns

welding gun was used for overall welding, so that the steel strip was completely welded to the steel tube (Fig. 5e, f).

### (3) Pouring concrete

The steel tube confined by FRP or steel strip was temporarily fixed to the bottom formwork through

hot melt adhesive, and the gap between the steel tube and bottom formwork was sealed with glass adhesive to prevent leakage of concrete during pouring, as shown in Fig. 6a. The concrete was prepared according to the proportion in advance and poured into the steel tube twice. A vibrating bar is used for artificial tamping (Fig. 6b, c).



(a) Fix on the bottom formwork



(b) Weigh raw material



(c) Pour and vibrate concrete



(d) Level the surface of concrete

**Fig. 6** Process of pouring concrete

Concurrently, a spatula or steel bar was inserted along the steel tube internal face many times to ensure that the interface between the steel tube and concrete was dense. Finally, a drawknife was used to level the surface of the concrete (Fig. 6d).

### 2.3 Material Properties

Three standard concrete cubes (150 mm × 150 mm × 150 mm) and three standard concrete prisms (Φ150 mm × 300 mm) were made to investigate the strength of the concrete used in this test. The average compressive strength of the concrete cube and concrete prisms was 32.4 MPa and 29.4 MPa, respectively.

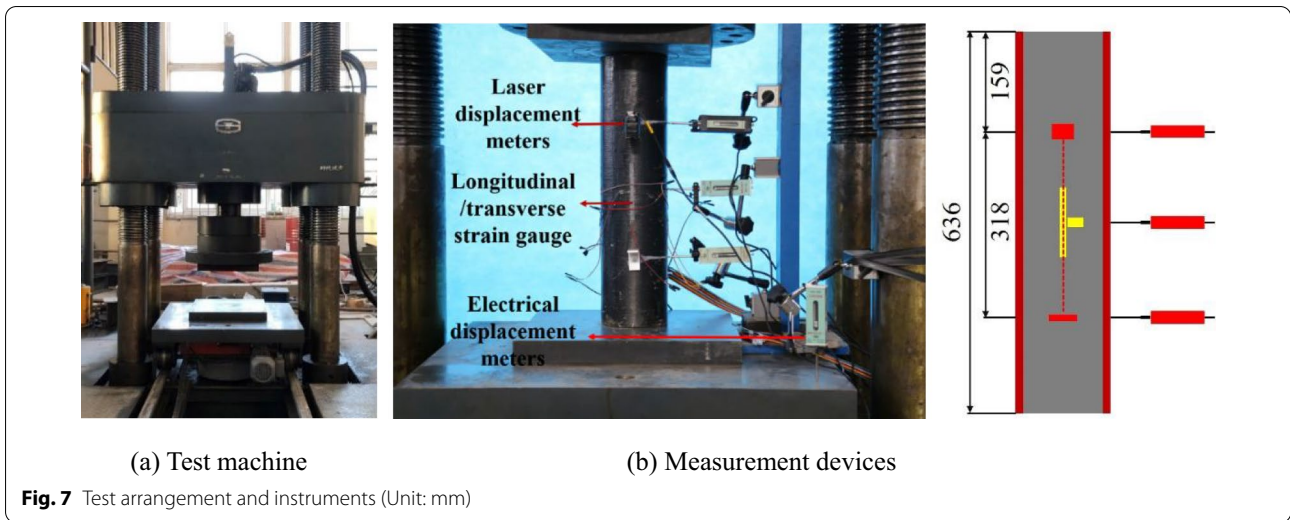
The thickness of the steel tube used in this test was 4.0 mm, the FRP used in this test was carbon fiber reinforced polymer, and the thickness of the steel strip was 3.0 mm and 6.0 mm. According to the Chinese code (GB/T 228.1–2010; GB/T 3354–2014), the material properties of the steel tube, FRP and steel strips were obtained by tensile testing on standard specimens. The average yield strengths of the steel tubes were 466.5 MPa. The average yield strengths of the steel

strips with thicknesses of 3.0 mm and 6.0 mm were 489.9 and 472.3 MPa. The ultimate tensile strength, ultimate tensile strain and elastic modulus of the FRP were 3406.4 MPa, 0.013 and 269.4 GPa.

### 2.4 Test Setup and Instrumentation

A microcomputer-controlled electrohydraulic servo pressure testing machine (YAW5000F), shown in Fig. 7a, was used to perform the axial compression test. One electrical displacement meter was placed on the bottom plate of the test machine to measure the overall deformation of the specimen. Two laser displacement meters were symmetrically placed on the middle of both sides of the specimens to measure the middle deformation of the specimens. Four pairs of longitudinal strain gauges and transverse strain gauges were installed on the middle of the specimens to measure the longitudinal strain and transverse strain of the specimens.

The specimen was preloaded before the formal loading. Preloading was performed three times. In each preloading



process, the axial load was increased to 50 kN and maintained for 3 min to eliminate the gap between the specimen and the test machine. In the formal test, displacement control was used, and the speed was 0.6 mm/min.

### 3 Results and Discussion

#### 3.1 Test Process and Failure Modes

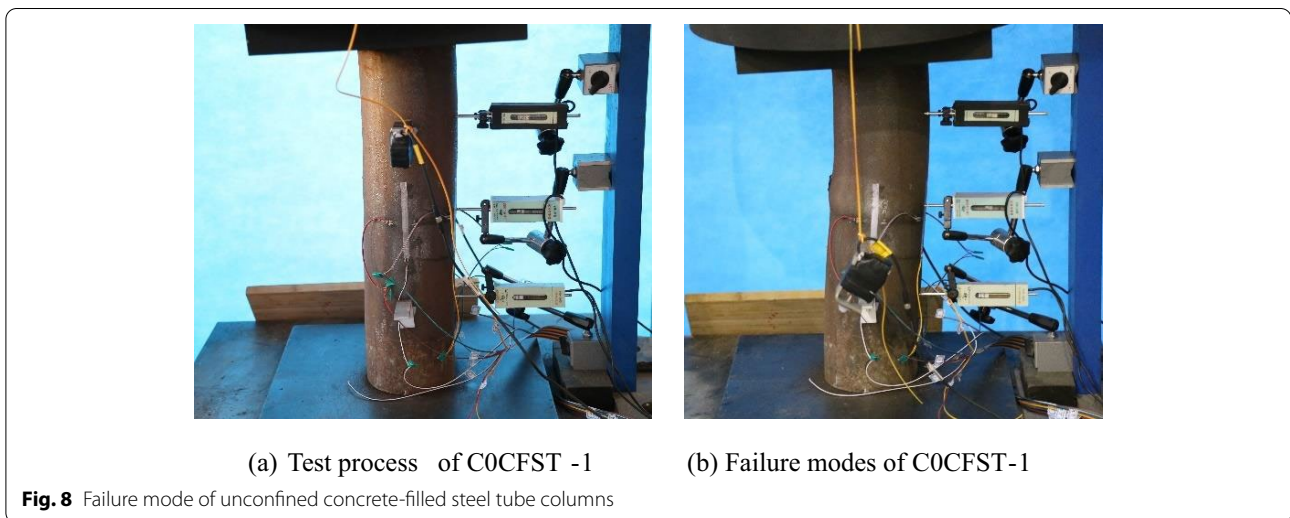
##### 3.1.1 Unconfined Concrete-Filled Steel Tube Columns

The test process and failure modes of unconfined concrete-filled steel tube columns (C0CFST series) are shown in Fig. 8. Considering specimen C0CFST-1 as an example, in the early stage of the test, the specimen was in an elastic state, and there was no marked phenomenon on the surface of the specimen. When the load reached 1346.2 kN, the rate of increase in the load began to

decrease, and the rust on the specimen surface began to fall off. After the axial load reached 1793.9 kN (i.e., the ultimate load), the axial load began to decline, and there was marginal buckling in the middle of the specimen. As the load continued to increase, buckling in the middle of the specimen became more pronounced, but the load nearly did not decrease.

##### 3.1.2 FRP-Strengthened Concrete-Filled Steel Tube Columns

The test process and failure modes of FRP-strengthened CFST columns are shown in Fig. 9. Considering specimen C2CFST-1 as an example, similar to the unconfined CFST columns, no marked phenomenon appeared on the surface of the specimen. When the axial load reached 1999.4 kN, the rate of increase in the load began



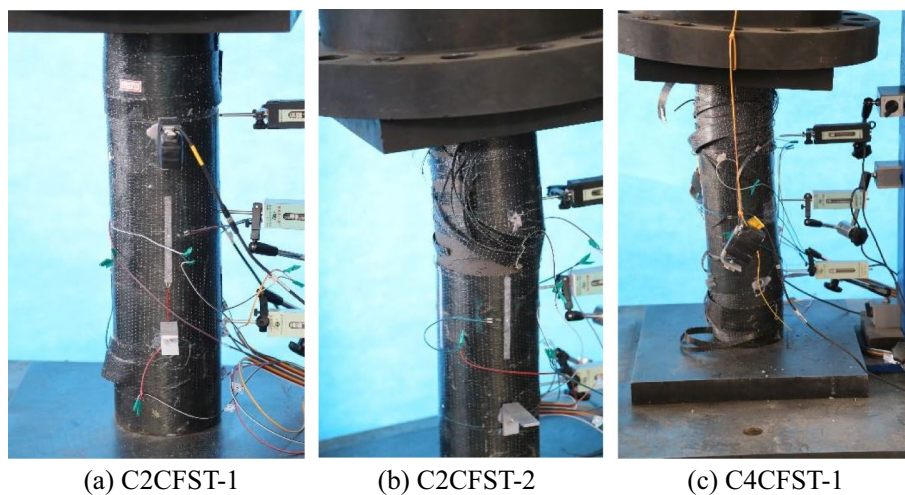


**Fig. 9** Failure mode of FRP-strengthened CFST columns

to decrease. There was a slight cracking sound of epoxy resin adhesive when the load reached 2286.2 kN. When the load reached 2392.5 kN, 2450.6 kN and 2545.8 kN, the FRP at the overlaps of the specimen broke several times. After the axial load reached the ultimate load (2600.6 kN), the load decreased markedly to 1999.4 kN, and the FRP fractured across a large area. As the specimen continued to be loaded, the FRP fracture became more serious and spread to the full height range of the specimen.

### 3.1.3 Welded Steel Strip-Strengthened Concrete-Filled Steel Tube Columns

The test process and failure modes of the welded steel strip-strengthened CFST columns are shown in Fig. 10. At the initial stage of loading, similar to the other two different structures, there is no marked phenomenon on the surface of the welded steel strip-strengthened CFST columns. As the load continued to increase, the rate of increase in the load began to decrease, and the rust on the surface of the specimens began to fall off. Then, the load increased linearly until it reached the ultimate load. In this process, the part of the specimen that was not reinforced by the steel strip began to bulge and gradually increased in size. Notably, the steel strip did not change during the whole loading process.

### 3.2 Axial Load–Strain Curves

The axial load–strain curves of all specimens are shown in Figs. 11 and 12. The longitudinal strain of the specimen is measured and corrected by the data from the electric displacement meter arranged at the lower edge of the test

machine, the displacement data of the testing machine itself and the longitudinal strain gauges set on the middle of the specimens. The hoop strain of the specimen is measured and corrected by the data from the transverse strain gauges set on the middle of the specimens.

Fig. 11 shows that the axial load–strain curves of the unconfined CFST column can be divided into three stages: elastic, yield and residual. In the elastic stage, the load increased linearly with increasing strain. Under the same load, the hoop strain of the specimen is smaller than the longitudinal strain. When the load increased to a certain value, the axial load–strain curves entered the yield stage, and the slope of the curve began to decrease slowly, which means that the steel tube began to yield. After the load reached the ultimate load, the curve began to show a downward trend and entered the residual stage. In the residual stage, the load did not decrease markedly, which demonstrates the superior ductility of CFST columns.

As shown in Fig. 12a–d, the axial load–strain curves of FRP-strengthened concrete-filled steel tube columns can be divided into four stages: elastic, elastic–plastic, strengthening, and residual. In the elastic stage, the load has a linear relationship with the longitudinal strain, and the stiffness of the specimen remains unchanged. Similar to the axial load–strain curves of unconfined CFST columns, the hoop strain is much smaller than the longitudinal strain of FRP-strengthened concrete-filled steel tube columns when the axial load is the same. After entering the elastic–plastic stage, the steel tube began to yield, the growth of the axial load tended to be slower than that in the elastic stage, and the longitudinal strain began to increase



**Fig. 10** Failure mode of welded steel strip-strengthened CFST columns

markedly. Then, the axial load–longitudinal strain curve enters the second linear growth stage. In the strengthening stage, the slope of the curve increases marginally until the FRP cracks, which indicates that FRP begins to

play a role in confining the core concrete in this stage. After the FRP breaks and the load reaches the ultimate load, the axial load decreases markedly. In the residual stage, each FRP fracture was accompanied by a marked decrease in load. However, the load remained at a certain value due to the constraint provided by the steel tube.

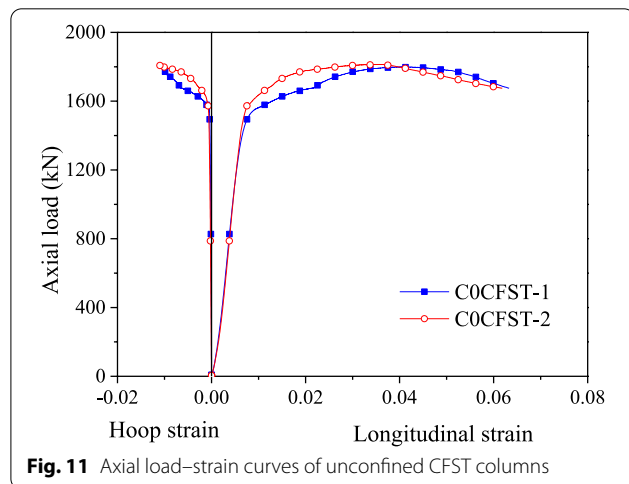


**Fig. 11** Axial load–strain curves of unconfined CFST columns

The axial load–strain curves of the welded steel strip-strengthened CFST columns are shown in Fig. 12e–f. Similar to the axial load–strain curves of the unconfined CFST columns, the axial load–strain curves of the welded steel strip-strengthened CFST column can also be divided into three stages: elastic, yield and residual. However, the primary difference between the axial load–strain curves of the welded steel strip-strengthened CFST column and unconfined CFST columns is that there is a longer linear growth stage that appears in the load–longitudinal strain curves of the welded steel strip-strengthened CFST column. However, the slope of this linear growth stage is markedly smaller than that of the strengthening stage of FRP-strengthened concrete-filled steel tube columns.

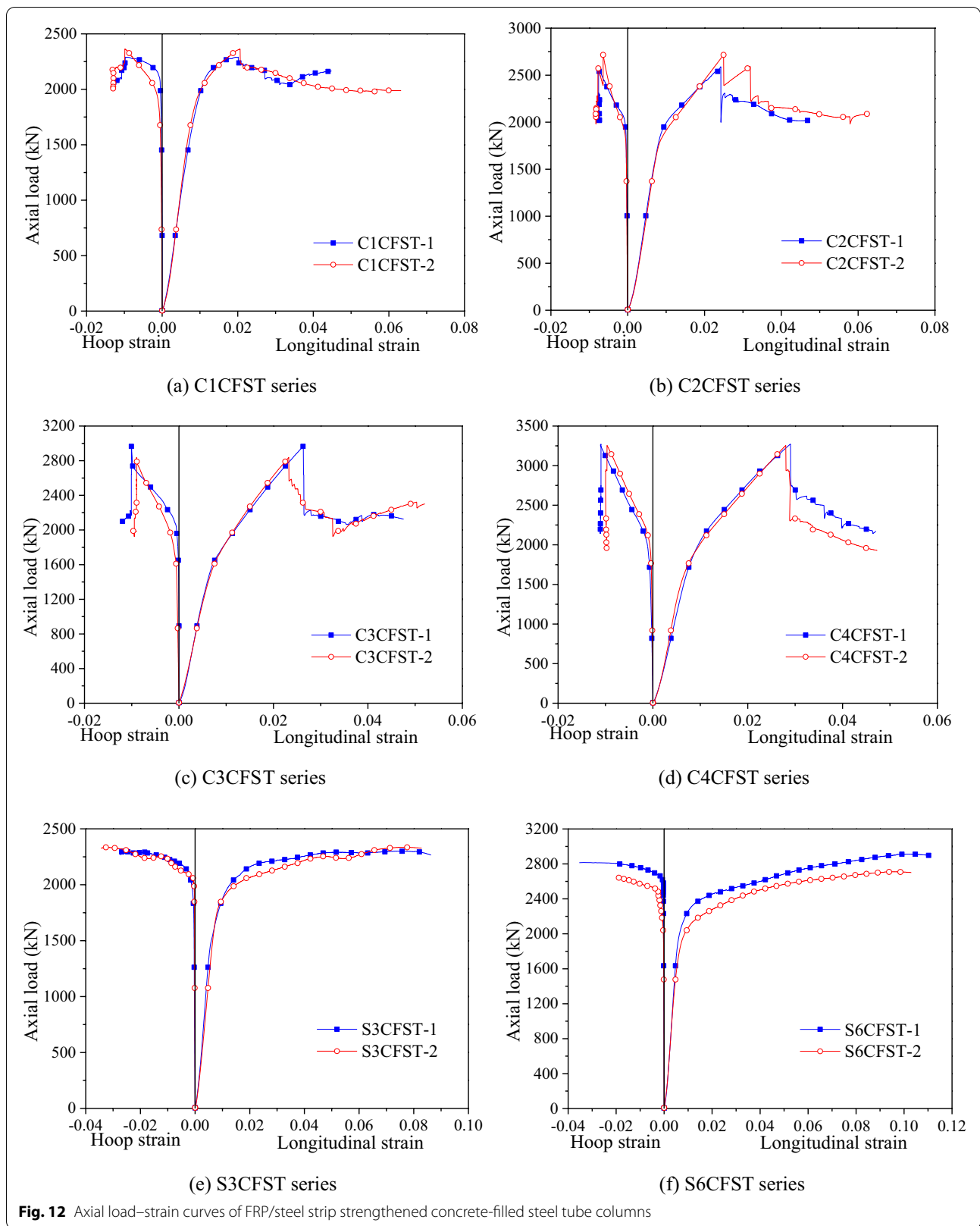
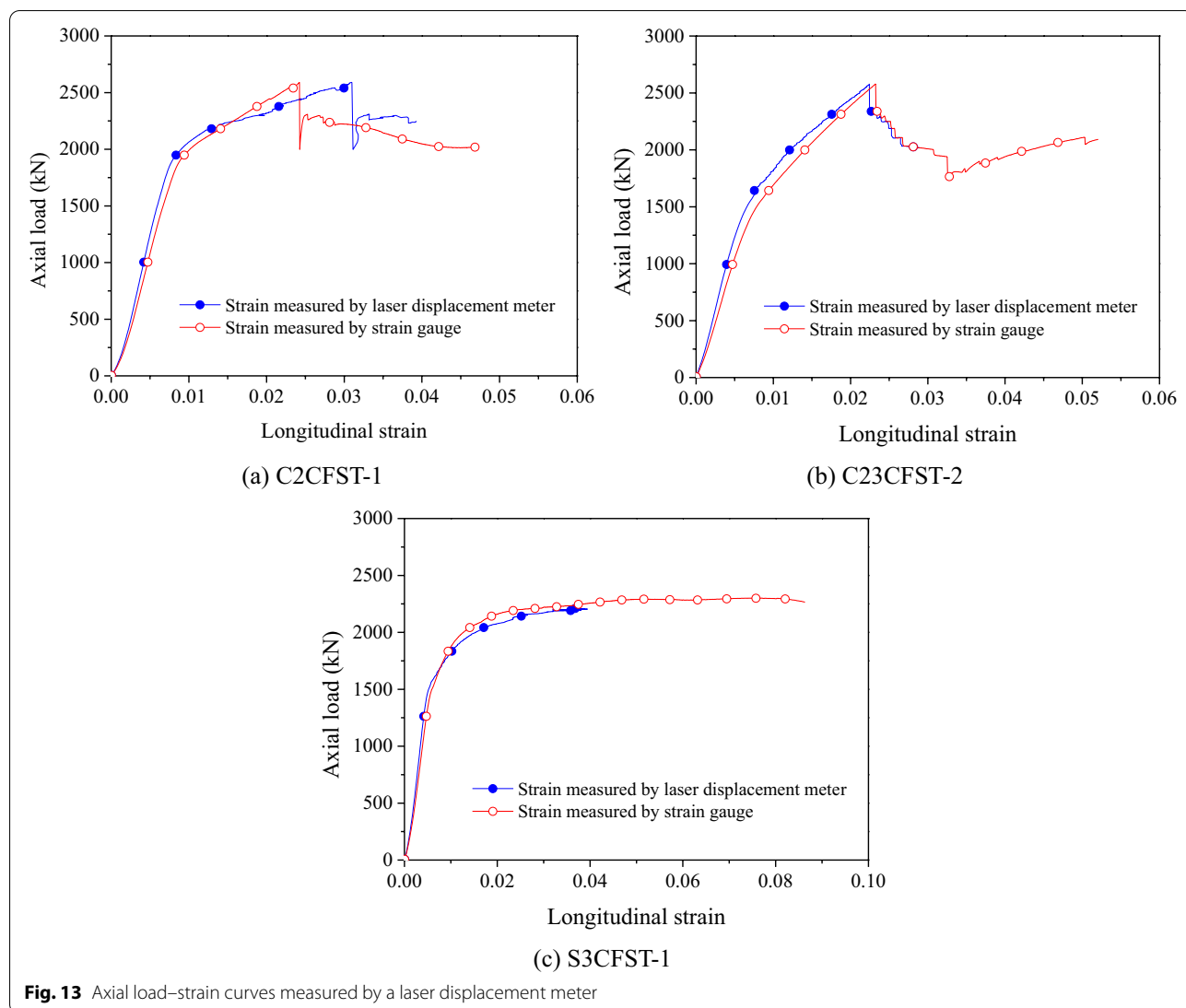


**Fig. 12** Axial load–strain curves of FRP/steel strip strengthened concrete-filled steel tube columns



The axial load–strain curves measured by the laser displacement meter are shown in Fig. 13. The *Y-axis* of the curve is the load value, and the *X-axis* is the longitudinal strain measured by the laser displacement meter or strain gauge, in which the strain measured by the laser displacement meter was obtained by dividing the deformation measured by the laser displacement meter by the distance (318 mm). The data measured by the laser displacement meter were interrupted when part of the specimen was damaged locally. Therefore, only some relatively complete axial load–strain curves were present in this paper. As seen from Fig. 13, the trends of the curves measured by the two different methods are almost identical. For the FRP-strengthened concrete-filled steel tube columns, the axial load–strain curves

were divided into four stages: elastic, elastic–plastic, strengthening, and residual. For the welded steel strip-strengthened CFST columns, the axial load–strain curves were divided into three stages: elastic, yield and residual.

### 3.3 Influence of Different Specimen Parameters

#### 3.3.1 Effect of FRP Layers

The influence of the number of FRP layers on the compression behavior of FRP-strengthened concrete-filled steel tube columns is shown in Fig. 14. Specimens C0CFST, C1CFST, C2CFST, C3CFST and C4CFST are concrete-filled steel tube columns confined by 0 layers, 1 layer, 2 layers, 3 layers and 4 layers of CFRP, respectively. As shown in Fig. 14a, the influence of FRP layers on the

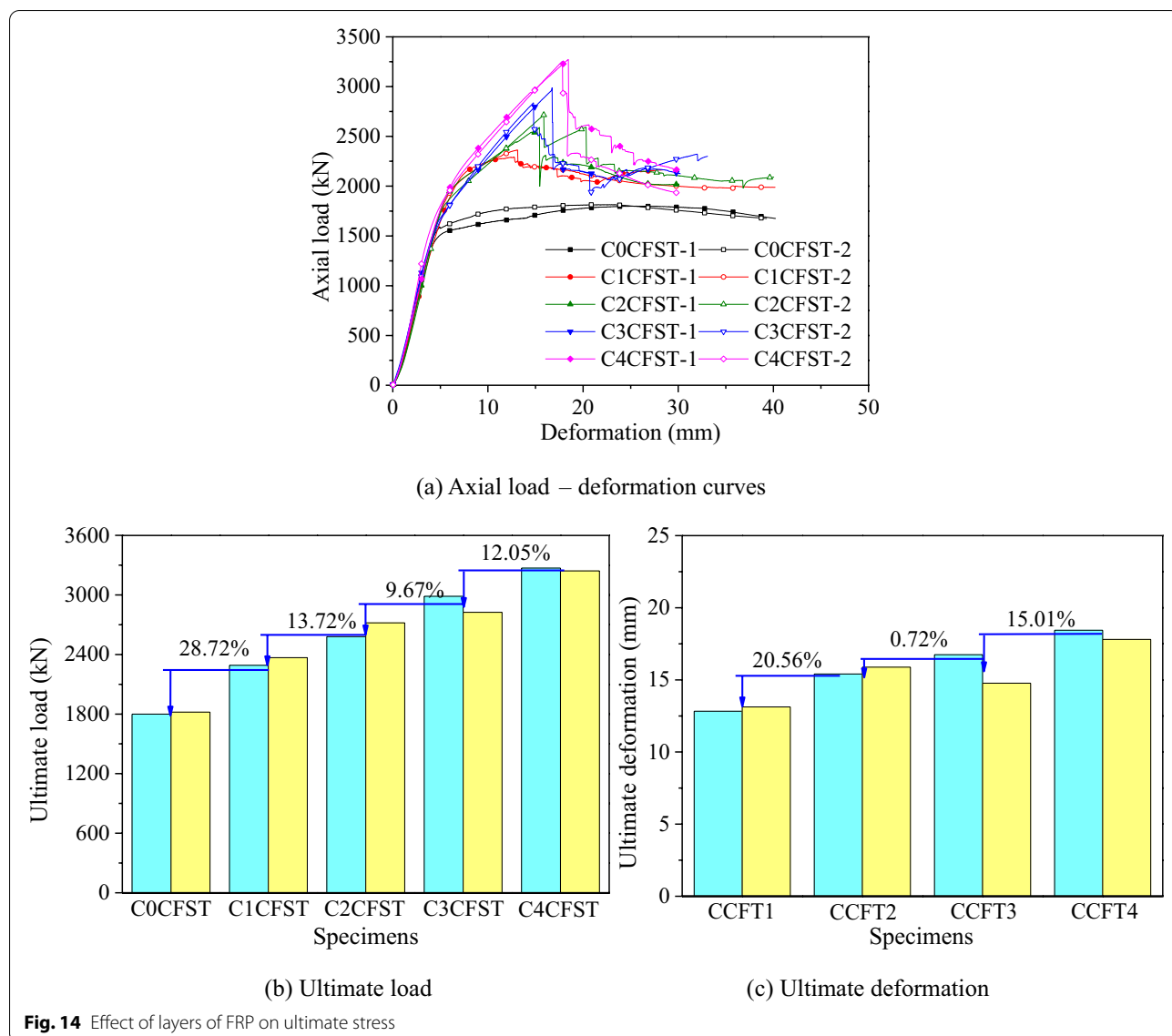


**Fig. 14** Effect of layers of FRP on ultimate stress

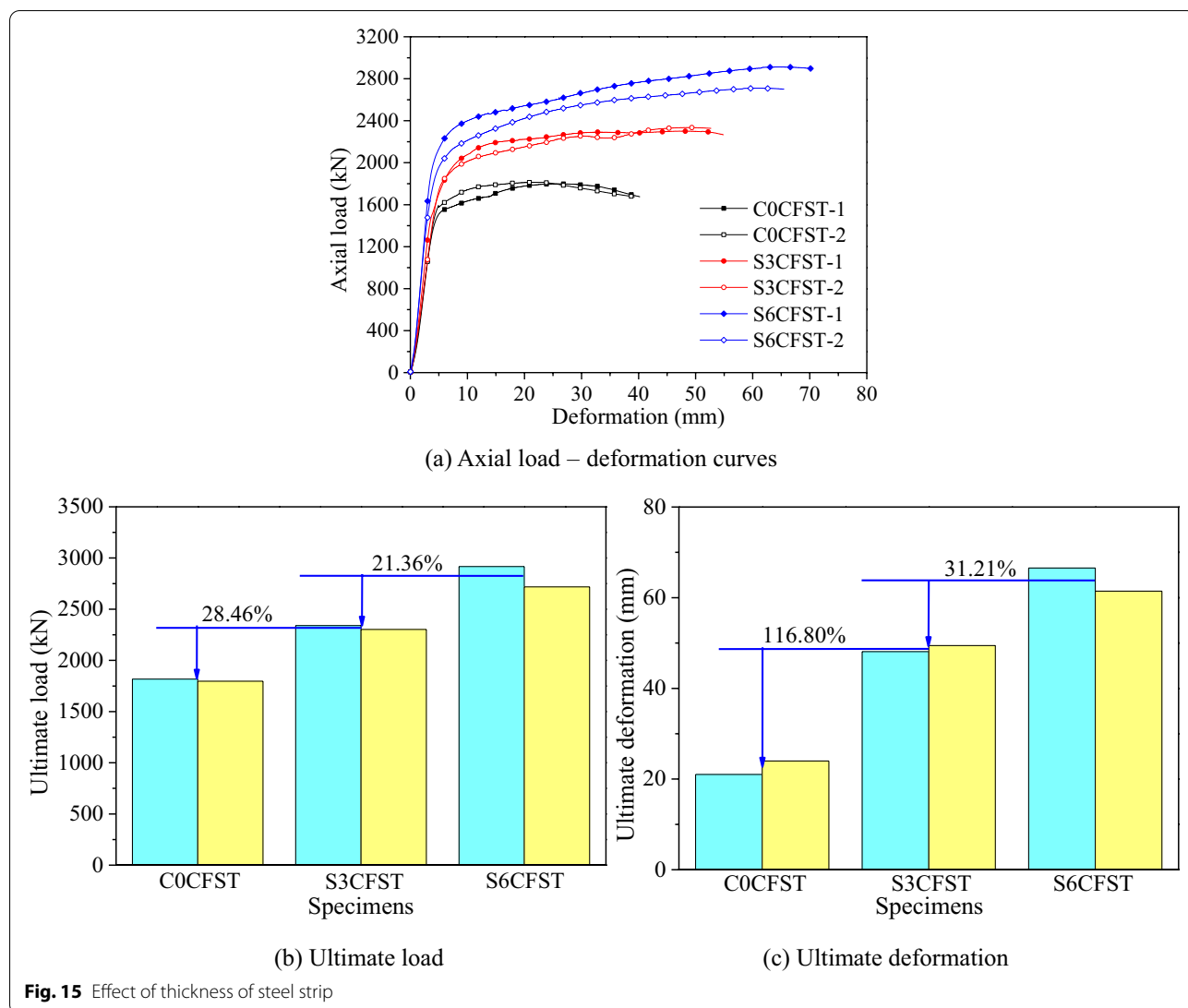
axial load–deformation curves of FRP-strengthened concrete-filled steel tube columns is primarily shown in the strengthening stage. The slope of the strengthening stage increases with the increase in the number of FRP layers, because a stronger constraint can be provided by more layers of FRP.

Fig. 14b, c shows that FRP can effectively improve the bearing capacity of concrete-filled steel tube columns. Compared with unconfined concrete-filled steel tube columns, the ultimate load of FRP-strengthened concrete-filled steel tube columns with one layer, two layers, three layers and four layers increases by 28.72%, 42.44%, 52.11% and 64.16%, respectively. The ultimate load and ultimate deformation also increased with more FRP layers. As the number of FRP layers increases from one to

four, the load-carrying capacity of FRP-strengthened concrete-filled steel tube columns increases by 9.67% to 13.72%, and the deformation capacity increases by 0.72% to 20.56%.

**3.3.2 Effect of Thickness of Steel Strip**

The influence of the thickness of the steel strip on the compression behavior of the welded steel strip-strengthened CFST columns is shown in Fig. 15. Specimens C0CFST, S3CFST, and S6CFST are unconfined concrete-filled steel tube columns, concrete-filled steel tube columns confined by steel strips with thicknesses of 3.0 mm and concrete-filled steel tube columns confined by steel strips with thicknesses of 6.0 mm.



**Fig. 15** Effect of thickness of steel strip

Fig. 15a shows that the setting of steel strips improves the stiffness of the structure, which is indicated by the slope of the initial stage of axial load–deformation curves of welded steel strip-strengthened CFST columns being larger than that of unconfined CFST columns. After the steel tube yielded, the curve of the welded steel strip-strengthened CFST columns showed a long linear growth stage, while the curve of unconfined CFST columns showed a downward trend earlier.

As shown in Fig. 15b, c, the bearing capacity and deformation capacity of the concrete-filled steel tube columns improved after being confined by the steel strip. The ultimate load of the welded steel strip-strengthened CFST columns increased by 28.46% and 49.82% when the thickness of the steel strip was 3.0 mm and 6.0 mm, respectively, compared with the unconfined CFST columns. The ultimate deformation

of the welded steel strip-strengthened CFST columns increased by 116.80% ~ 148.01% compared with the unconfined CFST columns. The ultimate load and ultimate deformation of the welded steel strip-strengthened CFST columns also improved with increasing thickness of the steel strip.

### 3.4 Comparison Between the CFRP and Steel Strip Strengthening Methods Based on the Consideration of Cost/Increase of Ultimate Load

To provide a reference for engineering practice, the cost performance of two different strengthening methods was compared by considering the cost/increase of ultimate load in this test.

The cost discussed in this section ignores labor costs, because labor costs vary markedly between different

**Table 3** Cost analysis of two different strengthening methods

Specimens	Increase of ultimate load/kN	Total cost of reinforcement/CNY	Cost/increase of ultimate load
C1CFST	519.80	$(80 + 56) \times 0.48 = 64.81$	0.12
C2CFST	839.35	$(80 + 56) \times 0.95 = 129.62$	0.25
C3CFST	1095.65	$(80 + 56) \times 1.43 = 194.43$	0.18
C4CFST	1446.00	$(80 + 56) \times 1.91 = 259.24$	0.18
S3CFST	514.06	$49.66 \times 0.48 = 23.84$	0.05
S6CFST	1009.98	$92.50 \times 0.48 = 44.40$	0.04

locations. Based on the local market, the costs of FRP, epoxy resin adhesive and 3.0/6.0 mm steel strips are 80 CNY, 56 CNY and 49.66/92.50 CNY per square meter. The costs of all FRP-strengthened CFST columns and welded steel strip-strengthened CFST columns in this test are listed in Table 3. The cost/increase of the ultimate load of CFST columns confined by FRP is lower than that of CFST columns confined by steel strips. Among the specimens in this test, CFST columns confined by steel strips with a 6.0 mm thickness are the most cost-efficient, with a cost/increase of ultimate load of 0.04. To achieve the same strengthening effect, the cost of the welded steel strip-strengthened CFST column is nearly 40% of that of the FRP-strengthened CFST column. Thus, welded steel strip-strengthened CFST columns are more cost-efficient than CFST columns confined by FRP.

Although welded steel strip-strengthened CFST columns are more cost-efficient, both reinforcement methods have advantages and disadvantages in engineering practice, and both can be applied to different projects. For the FRP confined method, the self-weight of the reinforced structure yields little increase in the structure's overall weight due to the FRP's low weight. Compared with welding steel strips, pasting FRP is more convenient for construction. For the welded steel strip confined method, cost performance is clearly the biggest advantage of this method. Compared with the FRP confined method, the construction technology of welded steel strips is more mature due to their longer development history.

## 4 Model for Ultimate Load of FRP/Welded Steel Strip-Strengthened CFST Columns

### 4.1 FRP-Strengthened CFST Columns

#### 4.1.1 Existing Models

- (1) Zhang et al.'s model (2019).

Zhang et al. (2019) collected 96 FRP-strengthened CFST columns under axial compression loads from

several different studies to establish a database. The model of the peak point and ultimate point were proposed by modifying and validating several researchers' models through the database. The calculation model for ultimate stress is as follows:

$$\frac{f_{cu}}{f_{co}} = 1 + 1.27\xi_s + 1.28\xi_f \quad (1)$$

where  $\xi_s$  and  $\xi_f$  are the confinement factors of the steel tube and FRP, respectively, and can be calculated as follows:

$$\xi_s = \frac{A_s f_y}{A_c f_{co}} \quad (2)$$

$$\xi_f = \frac{A_f f_f}{A_c f_{co}} = \frac{4E_f \varepsilon_f t_f}{f_{co} D} \quad (3)$$

where  $A_s$ ,  $A_f$  and  $A_c$  are the cross-sectional area of the steel tube, FRP and core concrete, respectively;  $f_y$  and  $f_{co}$  are the yield strength of the steel tube and the compressive strength of unconfined concrete, respectively; and  $E_f$ ,  $\varepsilon_f$ ,  $t_f$  and  $D$  are the elasticity modulus, ultimate tensile strain, thickness and diameter of FRP, respectively.

- (2) Tang et al.'s model (2020).

In 2019, Tang et al. (2020) conducted an axial compression test on 18 CFRP-confined concrete-filled stainless steel tube columns. The height–diameter ratio of all specimens is 3.5. The primary parameters of this test are steel tube thickness (3.0, 5.0 and 7.0 mm) and layers of CFRP (0, 1, 2, and 3 layers). Tang et al. (2020) proposed the growth index of bearing capacity  $\eta_{cap}$  to evaluate the influence of CFRP on the improvement of the bearing capacity of CFRP confined concrete filled stainless steel tube columns, which can be calculated by the following model:

$$\eta_{\text{cap}} = \frac{N_u - N}{N} \times 100\% \tag{4}$$

where  $N_u$  and  $N$  are the ultimate loads of the CFRP confined concrete filled stainless steel tube columns and unconfined concrete filled stainless steel tube columns, respectively.

Further analysis showed that the ultimate bearing capacity of CFRP-confined concrete-filled stainless steel tube columns increases linearly with the increase in the confinement factor ratio ( $\xi_f / \xi_s$ ) between the CFRP and stainless steel tubes. The relationship between the increasing index of bearing capacity  $\eta_{\text{cap}}$  and the confinement factor ratio ( $\xi_f / \xi_s$ ) is obtained by regression analysis:

$$\eta_{\text{cap}} = 0.42 \frac{\xi_f}{\xi_s} \tag{5}$$

Based on the above discussion, Tang et al. (2020) proposed a simplified calculation model for the ultimate load of CFRP-confined concrete-filled stainless steel tube columns:

$$N_u = (1 + \eta_{\text{cap}})(1.27FA_s + 0.85f_{\text{co}}A_c) \tag{6}$$

$$F = \min(f_y, 0.7f_u) \tag{7}$$

where  $f_u$  is the ultimate tensile strength of the steel tube.

(3) Lu et al.'s model (2014).

Lu et al. (2014) decomposed the ultimate bearing capacity ( $N_u$ ) of FRP confined concrete-filled steel tube columns into the ultimate load of steel tube  $N_s$ , the ultimate load of unconfined concrete ( $N_{\text{co}}$ ), the ultimate load of concrete under the circumferential constraint of steel tube ( $N_{\text{cs}}$ ) and the ultimate load of concrete under the circumferential constraint of FRP ( $N_{\text{cf}}$ ):

$$N_u = N_s + N_{\text{co}} + N_{\text{cs}} + N_{\text{cf}} \tag{8}$$

Based on the model for the ultimate load of concrete-filled steel tube columns proposed by Han et al. (2004) and the model for ultimate load of FRP confined concrete columns proposed by Yu et al. (2002), Lu et al. (2014) proposed the model for the ultimate load of FRP confined concrete-filled steel tube columns:

$$N_u = (1 + 1.8\xi_s + 1.15\xi_f)A_c f_{\text{co}} \tag{9}$$

(4) Ding et al.'s model (2018).

Ding et al. (2018) proposed that the ultimate load of FRP-confined concrete-filled steel tube columns can be divided into the longitudinal bearing capacity of steel tubes and the bearing capacity of concrete confined by FRP and steel tubes:

$$N_u = f_{\text{cc}}A_c + \sigma_{L,s}A_s \tag{10}$$

where  $f_{\text{cc}}$  is the compressive strength of concrete confined by the steel tube and FRP and  $\sigma_{L,s}$  is the longitudinal stress of the steel tube under axial loading, which can be calculated as follows:

$$\sigma_{L,s} = \left[ \sqrt{1 - \frac{3}{\xi_s^2} \left( \frac{\sigma_{r,c}}{f_{\text{co}}} - \frac{\xi_f}{2} \right)^2} - \frac{1}{\xi_s} \left( \frac{\sigma_{r,c}}{f_{\text{co}}} - \frac{\xi_f}{2} \right) \right] f_s \tag{11}$$

where  $\sigma_{r,c}$  is the circumferential binding force of concrete, which can be calculated as follows:

$$\sigma_{r,c} = \frac{\rho}{2(1 - \rho)} \sigma_{\theta,s} + \frac{\rho_1}{2(1 - \rho)} f_{\text{cf}} \tag{12}$$

where  $\sigma_{\theta,c}$  and  $f_{\text{cf}}$  are the circumferential binding force provided by the steel tube and the ultimate tensile strength of FRP, respectively;  $\rho$  is the ratio of the cross-sectional area of the steel tube and the sum of the cross-sectional areas of the steel tube and concrete; and  $\rho_1$  is the ratio of the sum of the cross-sectional areas of FRP and concrete and the sum of the cross-sectional areas of the steel tube and concrete.

By substituting Eqs. 11 and 12 into Eq. 10 and taking its derivative, Ding et al. (2018) suggested the following formula to predict the ultimate load of FRP-confined concrete-filled steel tube columns:

$$N_u = (1 + 1.7\xi_s + 1.7\xi_f)f_{\text{co}}A_c \tag{13}$$

(5) Tao et al.'s model (2007).

Tao et al. (2007) held the view that the ultimate bearing capacity of CFRP confined concrete-filled steel tube columns is closely related to the confinement factors of the FRP and steel tube.

For concrete-filled steel tube columns, the ultimate load of the model proposed by Han et al. (2004) was suggested:

$$N_u = (1.14 + 1.02\xi)f_{\text{ck}}A_{\text{sc}} \tag{14}$$

For FRP-confined concrete columns, the ultimate load of the model proposed by Yu et al. (2002) was suggested:

$$N_u = (1 + 1.15\xi_f)f_{co}A_c \tag{15}$$

Based on these models, Tao et al. (2007) proposed a model for the ultimate load of CFRP-confined concrete-filled steel tube columns by the regression analysis of experimental data:

$$N_u = (1 + 1.02\xi_s)f_{co}A_g + 1.15\xi_f f_{co}A_c \tag{16}$$

where  $A_g$  is the cross-sectional area of the steel tube and concrete.

(6) Hu et al.'s model (2014)

In 2014, Hu et al. (2014) believed that the ultimate bearing capacity of FRP-confined concrete-filled steel tube columns is the sum of the ultimate bearing capacity of steel tubes, the bearing capacity of concrete confined by steel tubes and the bearing capacity of concrete confined by FRP.

Thus, based on the model for ultimate load of FRP confined concrete columns proposed by Teng et al. (2007) and the model for ultimate load of concrete-filled steel tube columns proposed by Mander et al. (1988), the model for the ultimate bearing capacity of FRP confined concrete-filled steel tube column was proposed:

$$f_{cu} = \frac{f_{co}(1 + 3.5\frac{f_f}{f_{co}} + 2.254\sqrt{1 + \frac{7.94f_s}{f_{co}} - 2\frac{f_s}{f_{co}} - 2.254})A_c + \sigma_a A_s}{A} \tag{17}$$

**4.1.2 Validation of Existing Models**

Table 4 summarizes the three evaluation indices considered in this study—the average value (AV), the standard deviation (SD) and the average absolute error (AAE)—for the prediction accuracy of the above six models for the ultimate load of FRP-confined concrete-filled steel tube columns. As shown in Table 4, although the standard value and average absolute error of the Lu et al.'s model are good, the average value of the Lu et al.'s model is over 1.00, indicating that the Lu et al.'s model overestimates the bearing capacity of FRP-confined concrete-filled steel tube columns. The average values of the Tang et al.'s model and Tao et al.'s model are all below 1.00, which indicates that these two models underestimate the bearing capacity of FRP-confined concrete-filled steel tube columns. In contrast, the calculated values predicted by the Zhang et al.'s model, Ding et al.'s model and Hu et al.'s model are relatively

**Table 4** Evaluation results of existing models for FRP-strengthened CFST columns

Models	Average value (AV)	Standard deviation (SD), %	Average absolute error (AAE), %
Zhang et al.'s model	1.01	3.85	3.28
Tang et al.'s model	0.64	3.88	35.69
Lu et al.'s model	1.07	4.88	7.37
Ding et al.'s model	1.04	6.85	6.48
Tao et al.'s model	0.86	2.85	14.33
Hu et al.'s model	1.02	5.42	4.95

accurate. The standard deviation and average absolute error of these three models are 3.85%, 6.85%, and 5.42% and 3.28%, 6.48%, and 4.95%, respectively, indicating that the three models have good discreteness.

To analyze the accuracy of each model more intuitively, the comparison between the predicted value of the ultimate stress model and the experimental value is shown in Fig. 16. The horizontal and vertical coordinates are the experimental value and the calculated value of the ultimate stress, respectively. In Fig. 16, the three lines from top to bottom represent the error line and the ideal line, respectively, and the enclosed interval represents the error range.

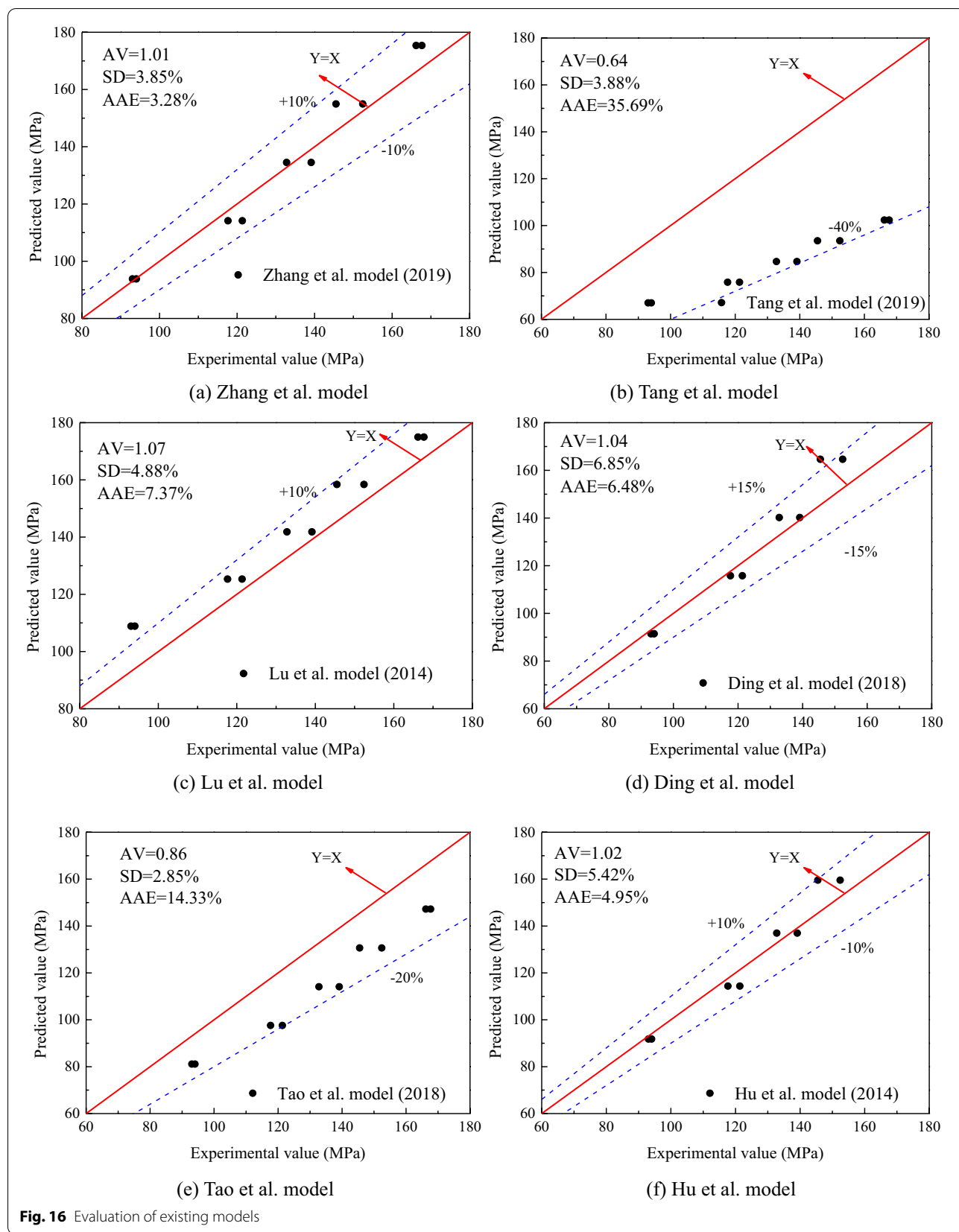
As shown in Fig. 16, the average value, standard deviation and average absolute error of the Tang et al.'s model and Tao et al.'s model are 0.64, 3.88%, 35.69% and 0.86,

2.85%, 14.33%, respectively. The error ranges of these two models both exceed -20%, indicating that the model underestimates the ultimate stress of the FRP-confined concrete-filled steel tube column. The Lu et al.'s model takes the circumferential constraint effect of the steel tube and FRP into consideration too much. The prediction results of the Zhang et al.'s model, Ding et al.'s model and Hu et al.'s model are thus the most satisfactory, and the error ranges of these three models are within  $\pm 10\%$ , while the discreteness of the Ding et al.'s model and Hu et al.'s model is worse than that of the Zhang et al.'s model.

**4.2 Welded Steel Strip-Strengthened CFST Columns**

**4.2.1 Proposed Model**

In this study, the ultimate strength of welded steel strip-strengthened CFST columns is considered to be the summation of the strength of core concrete confined by steel



tubes and steel strips and the longitudinal bearing capacity of the steel tube:

$$N = f_{cc}A_c + \sigma_a A_s \tag{18}$$

where  $\sigma_a$  is the longitudinal stress provided by the steel tube, which can be calculated by the following equation:

$$\sigma_a = \frac{1}{2} \left( \sigma_l - \sqrt{4f_y^2 - 3 \left( \frac{-0.42}{0.42 + \xi_s^{0.5} f_y} \right)^2} \right) \tag{19}$$

$f_{cc}$  is the strength of the core concrete confined by the steel tube and steel strips, which can be calculated by the model proposed by Mander et al. (1988):

$$f_{cc} = f_{co} \left( 1 + 2.254 \sqrt{1 + \frac{7.94 f_{ls}}{f_{co}} - 2 \frac{f_{ls}}{f_{co}} - 2.254} \right) \tag{20}$$

where  $f_{ls}$  is the lateral confinement provided by the steel tube and steel strip, which can be calculated by the following equations:

$$f_{ls} = f_{ls,st} + f_{ls,ss} = \frac{2t_{st}\sigma_{l,st}}{D_c} + \frac{2A_{ss}f_{y,ss}}{D_c s} \tag{21}$$

where  $A_{ss}$  is the steel strip cross-sectional area;  $f_{y,ss}$  is the yield stress of the steel strip;  $D_c$  is the diameter of the core concrete;  $s$  is the space of the steel strip; and  $\sigma_{l,st}$  is the hoop stress of the steel tube, which can be calculated by the model proposed by Wei et al. (2019b):

$$\sigma_{l,st} = \frac{-0.42}{0.42 + \xi_{st}^{0.5}} f_{y,st} \tag{22}$$

$$\xi_{st} = \frac{A_{s,st} f_{y,st}}{A_c f_{co}} \tag{23}$$

where  $A_{s,st}$  is the cross-sectional area of the steel tube and  $f_{y,st}$  is the yield stress of the steel tube.

### 4.2.2 Validation of Proposed Models

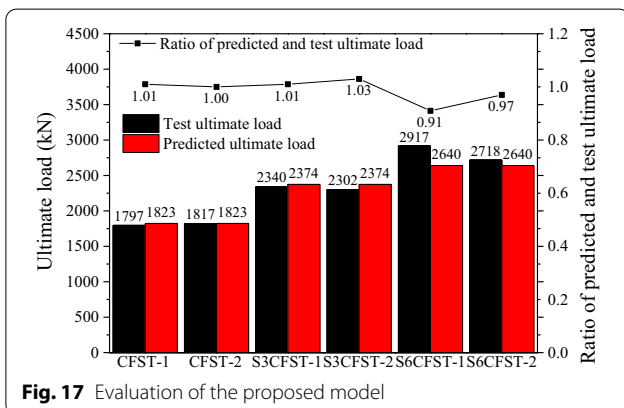
The validity of the proposed ultimate load models for welded steel strip-strengthened CFST columns was verified by comparing the experimental results with the predicted results. The comparisons are shown in Fig. 17. The average value of the proposed model is 0.99. The errors of most specimens are within 5%, except for specimen S6CFST-1, which may be caused by test errors. The standard deviation and average absolute error of the two models are 3.45% and 4.21%, respectively, which indicates that the two models can all accurately predict the ultimate load of both unconfined CFST columns and welded steel strip-strengthened CFST columns.

To the authors' knowledge, there is currently no calculation model for the bearing capacity of welded steel strip-strengthened CFST columns. The model proposed in this paper divides the bearing capacity of welded steel strip-strengthened CFST columns into two parts: the strength of core concrete confined by steel tubes and steel strips and the longitudinal bearing capacity of the steel tube. The strength of the core concrete confined by the steel tube and steel strips was calculated by the model proposed by Mander et al. (1988), while the longitudinal bearing capacity of the steel tube was calculated by Wei et al. (2019b). Compared with the existing models, the proposed model can calculate not only the ultimate bearing capacity of ordinary CFST columns but also the ultimate bearing capacity of welded steel strip-strengthened CFST columns, which shows the great universality of the proposed model.

### 5 Conclusions

Experimental and theoretical studies were conducted to investigate the compressive behavior of two different strengthening methods of concrete-filled steel tubes. FRP confined CFST and welded steel strip confined CFST. Based on the test results, the effect of FRP layers and steel strip thickness on the mechanical properties of FRP/welded steel strip-strengthened CFST columns was investigated. The cost performance of two different strengthening methods was also compared. Finally, the existing models for the ultimate load of FRP-strengthened CFST columns were concluded and evaluated. A model for the ultimate load of welded steel strip-strengthened CFST columns was also proposed. The following conclusions can be drawn:

- (1) The initial stage of the axial load–strain curves of the unconfined CFST columns, FRP-confined CFST columns and welded steel strip-strengthened CFST columns are nearly identical. After a yield stage, where the growth rate of the load decreased, the axial load–strain curves of the unconfined



CFST columns flattened out until the ultimate load was reached, after which the load began to decline slowly. The axial load–strain curves of FRP-strengthened CFST columns and welded steel strip-strengthened CFST columns entered a second linear strengthening stage until the ultimate load. Then, the load of FRP-strengthened CFST columns decreased sharply, while the load of welded steel strip-strengthened CFST columns decreased gradually.

- (2) Compared with unconfined CFST columns, the bearing capacity of FRP-confined CFST and welded steel strip-strengthened CFST columns markedly improved. Specifically, the ultimate load of FRP-strengthened CFST columns with one to four layers and welded steel strip-strengthened CFST columns with 3.0 mm and 6.0 mm steel strips increased by 28.72% to 64.16% and 28.46% to 49.82%, respectively. The deformation capacity improved with increasing FRP layers and steel strip thickness. Specifically, as the number of FRP layers increased from one to four, the deformation capacity increased by 0.72% to 20.56%. The deformation capacity increased by 31.21% when the steel strip thickness increased from 3.0 to 6.0 mm.
- (3) When the reinforcement effect of the two methods is similar, the cost of the welded steel strip-strengthened CFST column is nearly 40% of that of the FRP-strengthened CFST column. The cost performance of the welded steel strip-strengthened CFST column is better than that of the FRP-strengthened CFST column. Thus, considering only cost, welded steel strip-strengthened CFST columns are more suitable for engineering practice. However, considering the convenience of construction, FRP-strengthened CFST columns are more suitable.
- (4) Models of the ultimate load of FRP-strengthened CFST columns proposed by Zhang et al., Tang et al., Lu et al., Ding et al., Tao et al. and Hu et al. were evaluated. The average values of the Tang et al.'s model and Tao et al.'s model are 0.64 and 0.86, respectively, which indicates that these two models underestimate the restraint effect of FRP. Lu et al.'s model overestimates the bearing capacity of FRP-confined concrete-filled steel tube columns with an average value of 1.07. The model proposed by Zhang et al., Ding et al. and Hu et al. is relatively accurate and can be applied to the prediction of the ultimate load of FRP-strengthened CFST columns.
- (5) The ultimate load of the welded steel strip-strengthened CFST column is considered to be the sum of the strength of the core concrete confined by the steel tube and steel strips and the longitudinal bear-

ing capacity of the steel tube. Based on the Mander et al.'s model, a model for the ultimate load of a welded steel strip-strengthened CFST column was proposed and evaluated. From the evaluation results, the proposed model can be used to precisely calculate the ultimate load of welded steel strip-strengthened CFST columns and provide a reference for engineering practice.

#### Acknowledgements

The authors wish to express their gratitude to the National Natural Science Foundation of China (No. 51778300), Key Research and Development Project of Jiangsu Province (No. BE2020703), Natural Science Foundation of Jiangsu Province (No. BK20191390), 333 Project, Six Talent Peaks Project of Jiangsu Province (JZ-017), and Qinglan Project of Jiangsu Province for financially supporting this study.

#### Author contributions

SZ made a contribution to conduct the experimental test, analyze the test results and drafted the manuscript. KM made a contribution to conduct the experimental test and revised the manuscript. YW made a contribution to the conception and design of the work and revised the manuscript deeply. XX made a contribution to revise the manuscript. BL made a contribution to conduct the experimental test. WS made a contribution to conduct the experimental test. All authors read and approved the final manuscript.

#### Authors' information

Shichang Zhang is a Senior Engineer at Southeast University, Nanjing, China and Arcplus Institute of Shanghai Architectural Design and Research (Co., Ltd.), Shanghai, China.

Kunting Miao is a graduate student at the College of Civil Engineering, Nanjing Forestry University, Nanjing, China.

Yang Wei is a Full Professor in the College of Civil Engineering, Nanjing Forestry University, Nanjing, China.

Xiaoming Xu is a Senior Engineer in Arcplus Institute of Shanghai Architectural Design and Research (Co., Ltd.), Shanghai, China.

Bin Luo is a Full Professor at Southeast University, Nanjing, China.

Weizhou Shi is a Senior Engineer at the Arcplus Institute of Shanghai Architectural Design and Research (Co., Ltd.), Shanghai, China.

#### Funding

This investigation was supported by the following funders, and their role of the funding body was declared as follows:

1. The National Natural Science Foundation of China (No. 51208262): the design of the study;
2. The Key Research and Development Project of Jiangsu Province (No. BE2020703): collection of data;
3. The Natural Science Foundation of Jiangsu Province (No. BK20191390): analysis and interpretation of data;
4. Six Talent Peaks Project of Jiangsu Province (JZ-017) and Qinglan Project of Jiangsu Province: writing the manuscript.

#### Availability of data and materials

All data generated or analyzed during this study are included in this published article.

#### Declarations

#### Competing interests

No competing interests exist in the submission of this manuscript, and the manuscript has been approved by all authors for publication. The author declares that the work described is original research that has not been published previously and is not under consideration for publication elsewhere, in whole or in part.

**Author details**

<sup>1</sup>Southeast University, Nanjing 210096, China. <sup>2</sup>College of Civil Engineering, Nanjing Forestry University, Nanjing 210037, China. <sup>3</sup>Arcplus Institute of Shanghai Architectural Design & Research (Co., Ltd.), Shanghai 200041, China.

Received: 2 May 2022 Accepted: 22 August 2022

Published online: 02 January 2023

**References**

- Bradley, E. T., & Roberts, G. (2010). Crossing the Severn estuary, UK: challenges past and present. *Proceedings of the Institution of Civil Engineers Engineering History & Heritage*, 164, 123.
- Chin, C. L., Ma, C. K., Tan, J. Y., Ong, C. B., Awang, A. Z., & Omar, W. (2019). Review on development of external steel-confined concrete. *Construction and Building Materials*, 211, 919–931.
- China SP. (2010). Metallic materials tensile testing at ambient temperature vol GB/T 228.1–2010. Beijing
- China SPo. (2014). Test method for tensile properties of orientation fiber reinforced polymer matrix composite materials vol GB/T 3354—2014 Beijing
- Choi, K. K., & Yan, X. (2010). Analytical model of circular CFRP confined concrete-filled steel tubular columns under axial compression. *Journal of Composites for Construction*, 14, 125–133.
- Ding, F. X., Liu, Y. C., Fei, Y., Lu, D. R., & Chen, J. (2020). Cyclic loading tests of stirrup cage confined concrete-filled steel tube columns under high axial pressure. *Engineering Structures*, 221, 111048.
- Ding, F. X., Lu, D. R., Bai, Y., Gong, Y. Z., Yu, Z. W., Ni, M., & Li, W. (2018). Behaviour of CFRP-confined concrete-filled circular steel tube stub columns under axial loading. *Thin-Walled Structures*, 125, 107–118.
- Ekmekyapar, T., & Alhatmey, I. A. H. (2019). Post-fire resistance of internally ring stiffened high performance concrete filled steel tube columns. *Engineering Structures*, 183, 375–388.
- Feng, P., Cheng, S., Ba, I. Y., & Ye, L. (2015). Mechanical behavior of concrete-filled square steel tube with FRP-confined concrete core subjected to axial compression. *Composite Structures*, 123, 312–324.
- Han, L. H., Hou, C., & Wang, Q. L. (2012). Square concrete filled steel tubular (CFST) members under loading and chloride corrosion. *Experiments Steel Construction*, 71, 11–25.
- Han, L. H., & Yao, G. H. (2004). Experimental behaviour of thin-walled hollow structural steel (HSS) columns filled with self-consolidating concrete (SCC). *Thin-Walled Structures*, 42, 1357–1377.
- Hou, C. C., Han, L. H., Wang, Q. L., & Hou, C. (2016). Flexural behavior of circular concrete filled steel tubes (CFST) under sustained load and chloride corrosion. *Thin-Walled Structures*, 107, 182–196.
- Hu, H., & Seracino, R. (2014). Analytical Model for FRP-and-Steel-Confined Circular Concrete Columns in Compression. *Journal of Composites for Construction*, 18, 4013012.
- Hu, H. S., Xu, L., Guo, Z. X., & Shahrooz, B. M. (2020). Behavior of eccentrically loaded square spiral-confined high-strength concrete-filled steel tube columns. *Engineering Structures*, 216, 110743.
- K. Alrebeh S, Ekmekyapar T. (2019). Structural performance of short concrete-filled steel tube columns with external and internal stiffening under axial compression. *Structures*, 20, 702–716.
- Lai, M. H., & Ho, J. (2014a). Confinement effect of ring-confined concrete-filled-steel-tube columns under uni-axial load. *Engineering Structures*, 67, 123–141.
- Lai, M. H., & Ho, J. C. M. (2014b). Behaviour of uni-axially loaded concrete-filled-steel-tube columns confined by external rings. *Structural Design of Tall and Special Buildings*, 23, 403–426.
- Lai, M. H., & Ho, J. (2015). Axial strengthening of thin-walled concrete-filled-steel-tube columns by circular steel jackets. *Thin-Walled Structures*, 97, 11–21.
- Liao, F. Y., Han, L. H., & He, S. H. (2011). Behavior of CFST short column and beam with initial concrete imperfection: Experiments. *Journal of Constructional Steel Research*, 67, 1922–1935.
- Liao, F. Y., Han, L. H., & Zhong, T. (2013). Behaviour of CFST stub columns with initial concrete imperfection: Analysis and calculations. *Thin-Walled Structures*, 70, 57–69.
- Lu, Y. Y., Li, N., & Li, S. (2014). Behavior of FRP-Confined Concrete-Filled Steel Tube Columns. *Polymers*, 6, 1333–1349.
- Mander, J., & Priestley, M. (1988). Theoretical stress-strain model for confined concrete. *Journal of Structural Engineering*, 114, 1804–1826.
- Na, L., Lu, Y., Shan, L., & Lan, L. (2018). Slenderness effects on concrete-filled steel tube columns confined with CFRP. *Journal of Constructional Steel Research*, 143, 110–118.
- Stephens, M. T., Lehman, D. E., & Roeder, C. W. (2018). Seismic performance modeling of concrete-filled steel tube bridges: Tools and case study. *Engineering Structures*, 165, 88–105.
- Tang, H., Chen, J., Fan, L., Sun, X., & Peng, C. (2020). Experimental investigation of FRP-confined concrete-filled stainless steel tube stub columns under axial compression. *Thin-Walled Structures*, 146, 106483.
- Teng, J. G., Huang, Y. L., Lam, L., & Ye, L. P. (2007). Theoretical model for fiber-reinforced polymer-confined concrete. *Journal of Composites for Construction*, 11, 201–210.
- Wang, B., Liang, J., & Lu, Z. (2019). Experimental investigation on seismic behavior of square CFT columns with different shear stud layout. *Journal of Constructional Steel Research*, 153, 130–138.
- Wang, G., Wei, Y., Miao, K., Zheng, K., & Dong, F. (2022). Axial compressive behavior of seawater sea-sand coral aggregate concrete-filled circular FRP-steel composite tube columns. *Construction and Building Materials*, 315, 125737.
- Wang, Y. H., et al. (2021). Coupled ultimate capacity of CFRP confined concrete-filled steel tube columns under compression-bending-torsion load. *Structures*, 31, 558–575.
- Wang, Y., Cai, G., Larbi, A. S., Tsavdaridis, K. D., & Ran, J. (2020). Monotonic Axial Compressive Behaviour and Confinement Mechanism of Square CFRP-Steel Tube Confined Concrete. *Engineering Structures*, 217, 110802.
- Wei, Y., Bai, J. W., Zhang, Y. R., Miao, K. T., & Zheng, K. Q. (2021). Compressive performance of high-strength seawater and sea sand concrete-filled circular FRP-steel composite tube columns. *Engineering Structures*, 240, 112357.
- Wei, Y., Cheng, X., Wu, G., Duan, M., & Wang, L. (2019a). Experimental investigations of concrete-filled steel tubular columns confined with high-strength steel wire. *Advances in Structural Engineering*, 22, 2771–2784.
- Wei, Y., Jiang, C., & Wu, Y. F. (2019b). Confinement effectiveness of circular concrete-filled steel tubular columns under axial compression. *Journal of Constructional Steel Research*, 158, 15–27.
- Wei, Y., Zhu, C., Miao, K., Chai, J., & Zheng, K. (2022a). Compressive behavior of rectangular concrete-filled fiber-reinforced polymer and steel composite tube columns with stress-release grooves. *Composite Structures*, 281, 114984.
- Wei, Y., Zhu, C., Miao, K., Zheng, K., & Tang, Y. (2022b). Compressive performance of concrete-filled steel tube columns with in-built seawater and sea sand concrete-filled FRP tubes. *Composite Structures*, 281, 114984.
- Xu, B., Chen, H. B., Mo, Y. L., & Chen, X. M. (2017). Multi-physical field guided wave simulation for circular concrete-filled steel tubes coupled with piezoelectric patches considering debonding defects. *International Journal of Solids and Structures*, 122, 25–32.
- Yu, Q. (2002). *Behaviors of FRP-Confined Concrete Columns*. New York: Harbin Institute of Technology.
- Yu, T., Zhang, S., Huang, L., & Chan, C. (2017). Compressive behavior of hybrid double-skin tubular columns with a large rupture strain FRP tube. *Composite Structures*, 171, 10–18.
- Zeng, J. J., Lv, J. F., Lin, G., Guo, Y. C., & Li, L. J. (2018). Compressive behavior of double-tube concrete columns with an outer square FRP tube and an inner circular high-strength steel tube. *Construction and Building Materials*, 184, 668–680.
- Zeng, Y., Zhong, H., Liu, C., Tan, H., & Gu, A. B. (2017). Study of creep effects in a long-span concrete-filled steel tube arch bridge. *Proceedings of the Institution of Civil Engineers. Structures & Buildings*, 171, 1–17.
- Zhang, F., Xia, J., Li, G., Guo, Z., Chang, H., & Wang, K. (2020a). Degradation of Axial Ultimate Load-Bearing Capacity of Circular Thin-Walled Concrete-Filled Steel Tubular Stub Columns after Corrosion. *Materials*, 13, 795.
- Zhang, T., Zhu, H. H., Zhou, L., & Yan, Z. G. (2021). Multi-level micromechanical analysis of elastic properties of ultra-high performance concrete at high temperatures: Effects of imperfect interface and inclusion size. *Composite Structures*, 262, 113548.
- Zhang, Y., Wei, Y., Bai, J., Wu, G., & Dong, Z. (2020b). A novel seawater and sea sand concrete filled FRP-carbon steel composite tube column: Concept and behaviour. *Composite Structures*, 246, 112421.

- Zhang, Y. R., Wei, Y., Bai, J. W., & Zhang, Y. X. (2019). Stress-strain model of an FRP-confined concrete filled steel tube under axial compression. *Thin-Walled Structures*, 142, 149–159.
- Zhang, Y. F., & Zhang, Z. Q. (2015). Analysis on composite action of concrete-filled steel tube columns reinforced by different confining materials. *Materials Research Innovations*, 19, 236–239.
- Zheng, J., & Wang, J. (2017). Concrete-filled steel tube arch bridges in China. *Engineering*, 4, 143–155.
- Zhong, T., Han, L. H., & Zhuang, J. P. (2007). Axial Loading Behavior of CFRP Strengthened Concrete-Filled Steel Tubular Stub Columns. *Advances in Structural Engineering*, 10, 37–46.
- Zong, Z. H., Jaishi, B., Ge, J. P., & Ren, W. X. (2005). Dynamic analysis of a half-through concrete-filled steel tubular arch bridge. *Engineering Structures*, 27, 3–15.

### Publisher's Note

Springer Nature remains neutral with regard to jurisdictional claims in published maps and institutional affiliations.

Submit your manuscript to a SpringerOpen<sup>®</sup> journal and benefit from:

- ▶ Convenient online submission
- ▶ Rigorous peer review
- ▶ Open access: articles freely available online
- ▶ High visibility within the field
- ▶ Retaining the copyright to your article

---

Submit your next manuscript at ▶ [springeropen.com](https://www.springeropen.com)

---